Eur. Phys. J. B **27**, 7–10 (2002)
DOI: 10.1140/epjb/e20020124

THE EUROPEAN PHYSICAL JOURNAL B
EDP Sciences
© Società Italiana di Fisica
Springer-Verlag 2002

Secondary buckling patterns of a thin plate under in-plane compression

B. Audoly[1], B. Roman[2], and A. Pocheau[2,a]

[1] Laboratoire de modélisation en mécanique[b], Université Pierre et Marie Curie, 4 place Jussieu, 75252 Paris Cedex 05, France
[2] Institut de recherche sur les phénomènes hors d'équilibre[c], Universités Aix-Marseille I & II, 49 rue F. Joliot-Curie, BP 146, 13453 Marseille Cedex 13, France

Received 22 January 2002

Abstract. We study the nonlinear deformations of a long rectangular elastic plate clamped along its edges and submitted to in-plane biaxial compression. Using the Föppl–von Kármán equations, we predict various secondary buckling modes according to the applied longitudinal and transverse compressions. A model experiment is carried out in a thin polycarbonate film, and the observed buckling patterns are found in good agreement with theory. Pattern selection in the delamination of compressed thin films is discussed in the light of these results.

PACS. 46.32.+x Static buckling and instability – 68.55.-a Thin film structure and morphology – 89.75.Kd Patterns

Rapid Note

The way thin materials deform under the action of elastic stresses has proven to be of paramount importance in a number of phenomena standing at many different scales. These may be found in biophysics (*e.g.* membrane shape, vesicule conformation, retina detachment), mechanics (*e.g.* material resistance, film delamination) and geophysics (*e.g.* strata deformation), to cite but a few examples. However, current understanding of patterns displayed by thin elastic plates under stress is restricted to primary bifurcations (*e.g.* the initial buckling from the planar state) and simple primary structures (*e.g.* the Euler column, defined below) [1]. Despite recent advances in the strongly nonlinear regime [2,3], both the amplitude of deformation and the secondary instabilities of a plate at high stresses still resist analysis [4]. The difficulty comes from the presence of strong geometric nonlinearities in the theory of thin elastic bodies. As a result, the analysis of patterns is far less advanced in elasticity than in many other nonlinear systems [5].

This paper reports the first determination of the secondary instability diagram of a plane plate submitted to biaxial compression. Our approach consists in a joint experimental, theoretical and numerical study. A model experiment is conducted, in which primary buckling patterns are investigated, as well as secondary ones resulting from further instabilities. A theoretical analysis based on the Föppl–von Kármán equations (F.–von K.) is presented, which is complemented numerically using a Galerkin method. Altogether, these analyses build up the phase diagram of the strip. Incidentally, they establish that worm-like patterns allow an optimum release of the elastic energy in the context of thin film delamination [6].

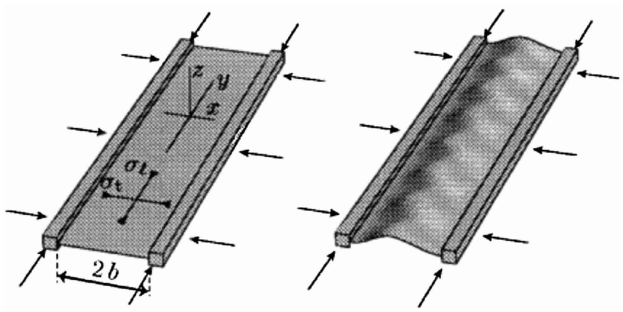

Fig. 1. A long elastic strip clamped along both sides is submitted to a biaxial in-plane compression (σ_t, σ_ℓ). This leads to buckling and postbuckling instabilities.

We consider a plane plate submitted to in-plane biaxial compression and to clamping boundary conditions (see Fig. 1). This geometry is a natural generalization of Euler's famous *Elastica* (the axially loaded rod). In contrast with the *Elastica*, both stretching and bending of the mean surface are important, and there is one additional space dimension. This will result in rather complex secondary buckling patterns, which we seek to evidence and determine.

Besides pattern formation, the studied system may also provide new insights into the delamination [7,8] of compressed thin films. It may indeed be regarded as a

[a] e-mail: alain.pocheau@irphe.univ-mrs.fr
[b] UMR 7607 du CNRS
[c] UMR 6594 CNRS

simple model of blister: biaxial compression accounts for the residual (thermal, chemical) film stresses driving delamination. The clamping boundary conditions are those for an elongated, straight blister. Note that coupling of film elasticity with fracture of the film/substrate interface are disregarded here, as the blister edges are fixed in advance. This simplification enables us to attack the post-buckling problem using the *exact* F.–von K. equations, instead of relying on controversial [3] approximations. There resides the main difference with former analyses of delamination blisters [8].

Buckling of the strip is described using the F.–von K. equations [1] for thin elastic plates:

$$D\,\Delta^2\zeta - h\left(\frac{\partial^2\chi}{\partial x^2}\frac{\partial^2\zeta}{\partial y^2} + \frac{\partial^2\chi}{\partial y^2}\frac{\partial^2\zeta}{\partial x^2} - 2\,\frac{\partial^2\chi}{\partial x\partial y}\frac{\partial^2\zeta}{\partial x\partial y}\right) = 0 \tag{1a}$$

$$\Delta^2\chi + E\left\{\frac{\partial^2\zeta}{\partial x^2}\frac{\partial^2\zeta}{\partial y^2} - \left(\frac{\partial^2\zeta}{\partial x\partial y}\right)^2\right\} = 0, \tag{1b}$$

where $D = E\,h^3/12(1-\nu^2)$, E is the Young's modulus of the film, h its thickness, ν its Poisson ratio, $\zeta(x,y)$ its deflection and $\chi(x,y)$ the Airy potential for the in-plane stress. The imposed biaxial in-plane compression [9] yields two additional terms $\sigma_{\rm t}\,\frac{\partial^2\zeta}{\partial x^2} + \sigma_\ell\,\frac{\partial^2\zeta}{\partial y^2}$ in equation (1a), where σ_ℓ (resp. $\sigma_{\rm t}$) denotes the applied stress in the longitudinal (resp. transverse) direction, as in Figure 1. Equations (1) are submitted to boundary conditions, not given here, expressing that the edges are clamped.

The compression applied on the edges of the plate has a destabilizing effect: to recover its natural length, the plate tends to buckle away from its rest plane, and bends. Buckling therefore results from a balance between the *release* of the in-plane compression energy — described by the last term in equation (1a) — and a *gain* of bending energy — the first term in this equation. Interestingly, this balance gives rise to many buckling bifurcations, addressed below.

The *linear* buckling of the plate has been solved for a long time [10] by an explicit linear stability analysis of the planar state $(\zeta,\chi) \equiv (0,0)$. Marginal stability is represented by the boundary of the P domain in the lower left-hand corner of Figure 2. When the *transverse* compression $\sigma_{\rm t}$ is dominant ($\sigma_\ell/\sigma_{\rm t} < 2/3$), the plate buckles to a cylindrical profile known as an "Euler column" (E domain). In this case, both the profile and the critical transverse load $\sigma_{\rm E}$ are simply given by Euler's Elastica: $\sigma_{\rm E} = \frac{E\,\pi^2}{12\,(1-\nu^2)}\left(\frac{h}{b}\right)^2$, b denoting half the strip width. When $\sigma_\ell/\sigma_{\rm t} > 2/3$, the plate bifurcates instead to a bump configuration (B domain). To our knowledge, this is the only known result on the buckling structures of the strip.

In the following, we complement this analysis of the primary bifurcation by considering compressions as large as several times $\sigma_{\rm E}$. It is consistent to use the F.–von K. equations to this end: their validity is not limited to a small dimensionless buckling parameter $\beta = [\max(\sigma_{\rm t},\sigma_\ell)/\sigma_{\rm E} - 1]$ but, instead [1], to small values of the combination $(h/b)\,\beta^{1/2}$. For a typical aspect ratio

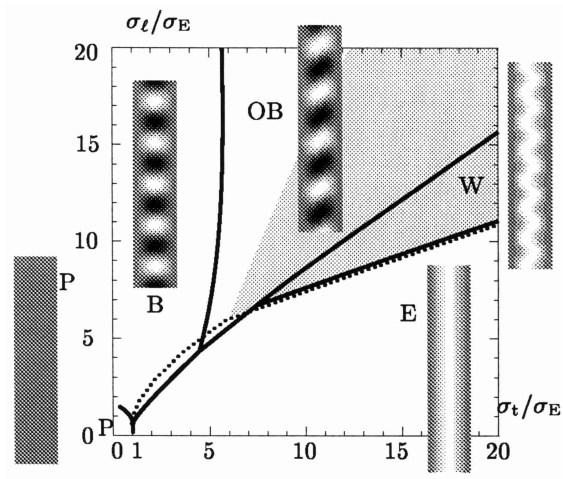

Fig. 2. Theoretical phase diagram for a film Poisson ratio $\nu = 0.3$. Thick lines delimit regions, in each of which the buckling mode of lowest energy is visualized using grey levels for the deflection ζ. Dotted line corresponds to marginal stability of the Euler column. Grey sector shows where the worm configuration is stable *or metastable*.

$h/b = 1/100$, the F.–von K. equations therefore remain valid for compressions as large as about $20\,\sigma_{\rm E}$.

We take advantage of the existence of an explicit, exact (although nonlinear) solution of the F.–von K. equations, the Euler column, and compute its linear stability. Extending a method discussed earlier in references [11,12], we indeed determine the locus in the $(\sigma_{\rm t},\sigma_\ell)$ plane where the Euler column becomes linearly unstable (dotted line in Fig. 2). In contrast, thick lines indicate a change in the configuration with minimum energy, as explained below. Dotted and thick lines coincide wherever the Euler column is the absolute minimum of energy *and* undergoes a supercritical bifurcation. This is actually the case for the Euler [E] to worms [W] transition. In contrast, the gap between these lines in the range $1 \le \sigma_{\rm t}/\sigma_{\rm E} \le 7.2$ indicates that the Euler column is no longer the absolute minimum of energy when it becomes unstable. This points out multistability of this system.

In order to further investigate the nonlinear buckling of the strip, we use a Galerkin procedure: we restrict the space of configurations of the plate to *three* modes of deformations. Guided by the analytical results reminded above, we choose them to be a cylindrical Euler like mode (E), a bump mode (+) symmetric with respect to $x \mapsto -x$ and an antisymmetric bump mode (−). The following form of the deflection was imposed:

$$\zeta(x,y) \;=\; v_{\rm E}\,\cos^2\frac{\pi\,x}{2\,b} + v_+\,\cos^2\frac{\pi\,x}{2\,b}\,\cos(k_+\,y) \tag{2}$$
$$\ldots + v_-\left(2\,\sin\frac{\pi\,x}{b} + \sin\frac{2\,\pi\,x}{b}\right)\cos(k_-\,y),$$

in agreement with the clamping conditions on the edges: $\zeta = \partial\zeta/\partial x = 0$ at $x = \pm b$. Equation (2) includes 5 trial parameters (3 amplitudes $v_{\cdot}$ and 2 wavenumbers $k_\pm$). The Airy potential was found in terms of these 5 parameters

Rapid Note

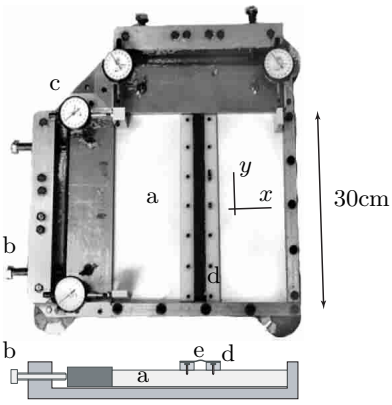

Fig. 3. Experimental set-up made up of a 30×30 cm^2 wide substrate (a) compressed along orthogonal directions using four screws (b), of four dial indicators (c) showing the imposed strain and of two rulers (d) screwed on the substrate, onto which the strip (e) is glued.

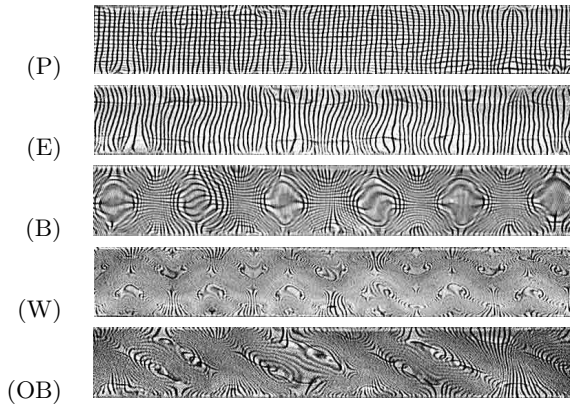

Fig. 4. Experimental buckling patterns identified from the distortion of a grid reflected on the strip surface (observed strip size is 20×150 mm^2): (P) initial level of distortion in the absence of buckling, (E) Euler column revealed by the separation of the longitudinal stripes, (B) bumps revealed by a symmetric distortion, (W) worms, (OB) oblique bumps.

by solving (1b), and the elastic energy was then calculated by combining χ and ζ. Minimization of this energy with respect to the 5 trial parameters was finally carried out. Resonances involving the symmetric and antisymmetric modes ($\pm$) were treated separately.

By varying the compressions $(\sigma_{\rm t}, \sigma_\ell)$, we obtained various buckling modes separated by bifurcations (thick lines in Fig. 2). These buckling modes are characterized by the set $\mathcal{S} = \{i \in \{\mathrm{E}, +, -\} \mid v_i \neq 0\}$ of indices of nonvanishing coefficients in equation (2): $\mathcal{S} = \{\mathrm{E}\}$ corresponds to Euler buckling (E), $\mathcal{S} = \{+\}$ to bumps (B), $\mathcal{S} = \{\mathrm{E}, -\}$ to worms (W), $\mathcal{S} = \{\}$ to the planar, unbuckled configuration (P). Oblique bumps (OB) are a *resonant* combination of the symmetric and antisymmetric modes: $\mathcal{S} = \{+, -\}$ and $k_+ = k_-$.

The experimental setup, shown in Figure 3, is designed to induce an homogeneous, biaxial compression in a polycarbonate strip. This is achieved by binding the strip to a thick $30 \times 30 \times 1$ cm^3 PVC block squeezed along two orthogonal directions independently (perpendicular and parallel to the film length) using screws. The strip is 295 mm long, 2 cm wide and 0.1 mm thick. It is not bound directly to the substrate but, instead, glued to small PVC rulers that are themselves screwed onto the substrate (Fig. 3, bottom). These rulers permit to transmit substrate compression to the strip while keeping it at a distance from the substrate so as to allow it to freely buckle. The substrate is chosen thick enough so as not to buckle during the experiment and to remain unperturbed by the film or the rulers: it acts as a reservoir of strain. It is moreover sucked downwards in such a way that is does not lift off the base at large in-plane compressions.

The main difficulty in this experiment comes from the presence of a small parameter, the film aspect ratio $h/2b = 5 \times 10^{-3}$, that enhances imperfections of the setup [14]. In-plane displacements of the film edge as small as $[2\,b \times \sigma_{\rm E}/E] \approx [2\,b\,(h/b)^2] \approx 2$ μm induce film stresses of order $\sigma_{\rm E}$, *i.e.* are large enough to make the film buckle. This makes the setup extremely sensitive to mechanical gaps (*e.g.* between base and substrate) and to the quality of the ruler-film binding. Still because of the small parameter h/b, temperature variations of only 2 K induce thermal stresses of order $\sigma_{\rm E}$: the setup had to be put in a temperature controlled box.

The applied stresses $(\sigma_{\rm t}, \sigma_\ell)$ were deduced from the compression-induced shortening of the substrate, measured by four indicators with micrometric accuracy. Experimental accuracy is assessed as follow. The amplitude of the mechanical gaps is estimated from the hysteresis in the output of the indicators following a typical, large cycle of loading: about 2 μm. The quality of the initial state of the strip is estimated from the slight distortions in the snapshot labeled 'P' in Figure 4: they amount to an initial unwanted stress of order (but not larger than) $\sigma_{\rm E}$. This gives rise to overall errors of the order $\sigma_{\rm E}$ on $(\sigma_{\rm t}, \sigma_\ell)$. This systematic error is acceptable since experiments are meant to explore the strongly nonlinear regime.

The buckling structure of the strip was determined from the distortions of the image of a grid reflected on the strip surface. The observed patterns, shown in Figure 4, remarkably coincide with those predicted by the theory. In particular, the existence of a (resonant) oblique bump mode (OB) was confirmed. Near the transitions, pattern identification was improved by performing image differences (Moiré effect). The experimental phase diagram is reported in Figure 5. Observations are limited to an angular sector due to the Poisson ratio of the film [13] and the sampling interval between measurements is $2\sigma_{\rm E}$, *i.e.* twice the experimental accuracy. Bistability, denoted using twin symbols, corresponds to the observation of either oblique bumps or worms depending on the loading history or on external perturbations.

Discrepancies between theory and experiments can arise from: (i) mechanical gaps amplified by the small factor h/b, as discussed above; (ii) the nonzero deformation threshold needed for pattern identification; (iii) the

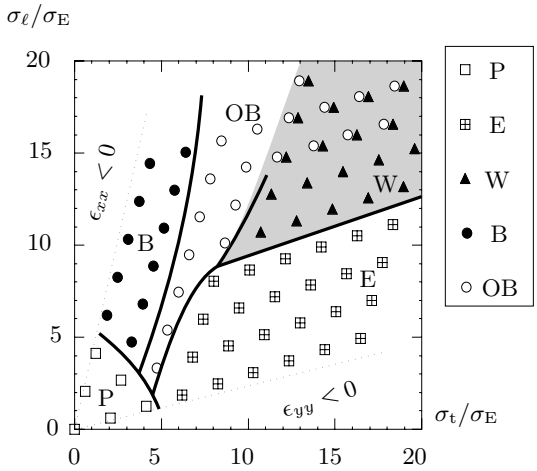

Fig. 5. Experimental phase diagram: observation of the patterns in Figure 4 is reported using symbols. Legend is otherwise as in Figure 2. Note the bistability region with both oblique bumps and worms. Comparison with the theoretical phase diagram (Fig. 2) involves no adjustable parameter.

finite strip length, which, by inhibiting potentially unstable wavenumbers $k_\pm$ stabilizes the planar state; (iv) multistability. Factors (i–iii) contribute to an overall experimental error of order σ_E (one unit in the diagrams): the P domain is enlarged in the experimental diagram compared to the theoretical one by (i) and (iii), and an overall offset of the experimental diagram toward higher stresses is induced by (i). Multistabilty (iv) is an actual *feature* of the system, and is *not* due to a limited experimental accuracy. It has been observed both experimentally and numerically.

Despite the above difficulties, one obtains a good overall agreement between the experimental and theoretical diagrams. In particular, the relative positioning of the various patterns is identical (Figs. 2 and 5). Such an agreement is remarkable given that strongly nonlinear regimes ($\sigma_{t,\ell}/\sigma_E \sim 20$) are being investigated. We should also emphasize that, in a multistable system as this one, comparison of the location of the transition lines does not necessarily make sense, because experimental transitions are triggered by perturbations that are difficult to control. The overall shape of the diagram is therefore more relevant than the precise location of the bifurcations. For instance, the observed worm domain W in Figure 5 is wider than expected from a mere minimization of energy (thick lines in Fig. 2); the essential point, however, is that is lies within the region of metastability predicted by theory (grey sector in Fig. 2).

This phase diagram of a compressed elastic strip provides a new understanding of the telephone cord (also called worm like) patterns observed in thin-films blistering. At large, isotropic compressions ($\sigma_t = \sigma_\ell$), as in temperature driven delamination, the diagram exhibits two equilibrium configurations (Figs. 2 and 5): oblique bumps (OB) and worm (W). The former, OB, has a slightly lower energy but is forbidden in delamination, as it violates the condition of non-interpenetrability with the substrate, $\zeta > 0$ [15]. Telephone cord patterns therefore emerge from the present analysis as a mean to minimize the elastic energy of the film. Such a variational selection accounts for the existence of worm like patterns, whose origin has remained rather obscure since they were first observed almost 40 years ago [6].

In addition, it has recently been reported [16] that worm like or straight patterns can be reversibly transformed into varicose ones by tuning transverse compression; this can be understood from the presence of bumps (B) and worms (W) besides oblique bumps (OB) in the upper part of diagram.

We have investigated the secondary buckling patterns of a long rectangular elastic plate submitted to biaxial in-plane compression. The instability domains, the marginal stability lines and the domains of multistability have been characterized by nonlinear theoretical analysis, numerical Galerkin method and a model experiment. Altogether, these analyses revealed a remarkably complex phase diagram for such a simple system. Incidentally, at large isotropic compressions and for an impenetrable substrate, the energy of the film was shown to be best released by worm like patterns. This provides a simple selection mechanism for the telephone cord blisters observed in thin film delamination.

We are very grateful to Yves Pomeau for stimulating discussions.

References

1. L.D. Landau, E.M. Lifschitz, *Theory of Elasticity* (Pergamon Press, New York, 1986).
2. Y. Pomeau, Phil. Mag. B **78**, 235 (1998).
3. W. Jin, P. Sternberg, J. Math. Phys. **42**, 192 (2001).
4. E.A. Thornton, Appl. Mech. Rev. **46**, 485 (1993).
5. M.C. Cross, P.C. Hohenberg, Rev. Mod. Phys. **65**, 851 (1993).
6. J.R. Priest *et al.*, in *Trans. of the Ninth National Symp. of the Amer. Vacuum Soc.*, edited by G.H. Bancroft (MacMillan, 1962), p. 201.
7. G. Gille, B. Rau, Thin Solid Films **120**, 109 (1984).
8. G. Gioia, M. Ortiz, Adv. Appl. Mech. **33**, 119 (1997).
9. Buckling is displacement controlled and not stress controlled: $\sigma_{t,\ell}$ refer to *residual* film stresses in delamination.
10. S. Timoshenko, J.M. Gere, *Theory of Elastic Stability*, 2nd edn. (MacGraw Hill, New York, 1961).
11. H.M. Jensen, Acta Metal. Mater. **41**, 601 (1993).
12. Basile Audoly, Phys. Rev. Lett. **83**, 4124 (1999).
13. Indicators output *strains* ϵ_{xx} and ϵ_{yy} that are linear combination of σ_t and σ_ℓ involving ν.
14. See *e.g.* N. Yamaki, J. Appl. Mech. **26**, 407 (1959).
15. B. Audoly, B. Roman, in preparation.
16. M. George, C. Coupeau, J. Colin, F. Cleymand, J. Grihlé, Phil. Mag. A **82**, 633 (2002)